Research Report

98-33

Axial Flux Circumferential Current Permanent Magnet (AFCC) Machine

J. Luo, D. Qin, T.A. Lipo, S. Li*, S. Huang**

Wisconsin Power Electronic Research Center
University of Wisconsin-Madison
Madison WI 53706-1691

*Beijing Inst. of Control Devices
P.O. Box 3913-23
Beijing 100039
P.R. China

**Shanghai University
147 Yan-Chang Road
Shanghai, 200072
P.R. China

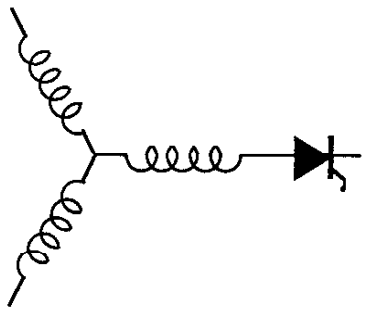

Wisconsin
Electric
Machines &
Power
Electronics
Consortium

University of Wisconsin-Madison
College of Engineering
Wisconsin Power Electronics Research Center
2559D Engineering Hall
1415 Engineering Drive
Madison WI 53706-1691

Axial Flux Circumferential Current Permanent Magnet (AFCC) Machine

Jian Luo Dinyu Qin Thomas A. Lipo Shuxiang Li* Surong Huang**
Student Member, IEEE Fellow, IEEE

Department of Electrical & Computer Eng.
University of Wisconsin-Madison
1415 Engineering Drive,
Madison, WI 53706
Tel: (608)-262-0287 Fax: (608)-262-1267
Email: luoj@cae.wisc.edu, qin@cae.wisc.edu, lipo@engr.wisc.edu

*Beijing Institute of Control Devices
P. O. Box 3913-23
Beijing 100039
P. R. China
Tel: 86-10-68764814

**College of Automation
Shanghai University
147 Yan-Chang Road,
Shanghai,200072,P.R .China
Tel: 86-21-62755573
Email: srhuang@yc.shu.edu.cn

***Abstract*-Based on the concept of the converter fed machines (CFMs), high power density machines with non-sinusoidal current and back emf waveforms are attracting more and more research interest. In this paper, a novel type of axial flux circumferential current permanent magnet (AFCC) machine topology is introduced. A sizing equation analysis, finite element analysis, optimization of parameters, performance simulation, details of the prototype and test data are included. In addition, a comparison of the power densities between the AFCC machine and the traditional induction machine based on the sizing and power density equations is also provided. Alternative manufacturing arrangements and the method to reduce torque ripple are discussed.**

I. INTRODUCTION TO THE AFCC MACHINE

Traditional design of an AC electrical machine assumes the presence of a sinusoidal voltage source resulting in a consequent sinusoidal back emf and sinusoidal current in the machine. It was recognized in [1]-[3] that the emergence of power electronic converters has removed the need for such a concept as the basis for machine design. Further, it has been shown that in order to enhance power density, rectangular waveforms of back emf and current is desirable.

Beginning with the switched reluctance machine (SRM) [4] and doubly-salient permanent-magnet machine (DSPM) [5] [6], an increasing level of interest has been paid to such non-traditional machines to achieve higher power density. For example, the claw-pole machine has attracted some re-attention [7] and improvements have been achieved with concepts such as transverse flux machine (TFM) [8]. As mentioned in [9], this kind of machine has an unusual property. That is, the power density can be increased by an increase in the pole number while the speed remains unchanged. In other words, the torque capability can be increased by simply increasing the pole number of the machine. However, limits exist (such as the leakage between poles with different polarity, rotating magnets, complexity of the structure) which still requires further research. In this paper, a novel type of AFCC machine topology is introduced to attempt to avoid such limitations.

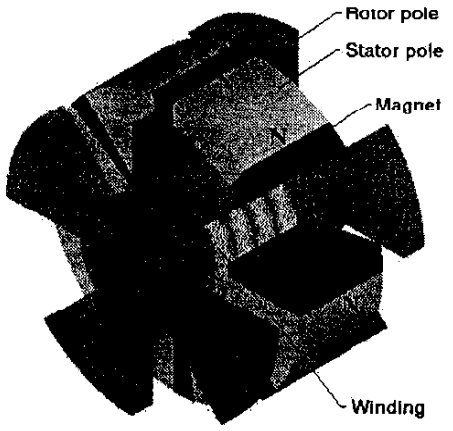

Fig. 1 An AFCC Machine

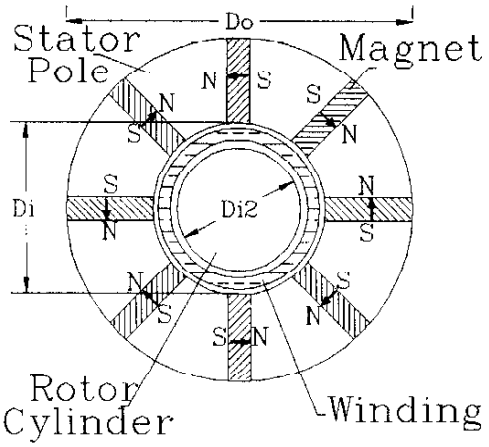

Fig. 2 Two Dimensional view of an AFCC machine.

In essence, AFCC machine is a new realization of the doubly salient permanent magnet machine structure reported previously [3]. As shown on Figs. 1, and 2, an AFCC machine consists of three parts, a stator with iron poles and

permanent magnets (PMs), a circumferential armature winding, a rotor with salient poles and a center cylindrical portion. The main flux provided by two nearby PMs are focused in the stator pole and become axially oriented when passing across the gap. The flux then passes the air-gap, the rotor pole, the rotor cylinder, the rotor pole on the other side and returns to the next stator pole. The rotor poles on the two end plates are shifted by one pole pitch. For a generator application, a rotating rotor causes the flux linked by the winding to be reversed periodically to generate a back emf. For a motor application, an injected current will then create a reluctance torque. It should be noted that the rotor and stator of the AFCC machine can be interchanged depend on the specific application. However it is preferred that the armature winding always be mounted to the stationary part in order not to rotate.

Because the main flux path in the AFCC machine has a complicated three dimensionally distribution, the material of the stator pole and rotor must be tailored to meet such a situation. For this purpose, novel materials such as powdered metal could be utilized for manufacturing. On the other hand, the AFCC machine can also be constructed with traditional laminated silicon-iron to reduce the cost. Fig. 3 illustrates one of the possible arrangements.

The AFCC machine has many of the attractive features that motor designers desire. Specifically the topology eliminates the end-winding portion to provide less copper losses and reduce leakage. It has stationary, not rotating, magnets to eliminate the excitation penalty. It has a strong flux focusing capability, which allows the use of low cost material such as ferrite magnets. The approach also has bipolar rather than unipolar (pulsating) phase flux even though the magnets are not rotating. Other features include simple armature winding construction, tape wound stator core and high pole number capability with low aspect ratio.

Table I shows a comparison of features among AFCC, induction machine, SRM, DSPM, flux-reversal machine (FRM) [10], a brushless DC machine (BLDCM) and the traditional claw pole machine (CLAW).

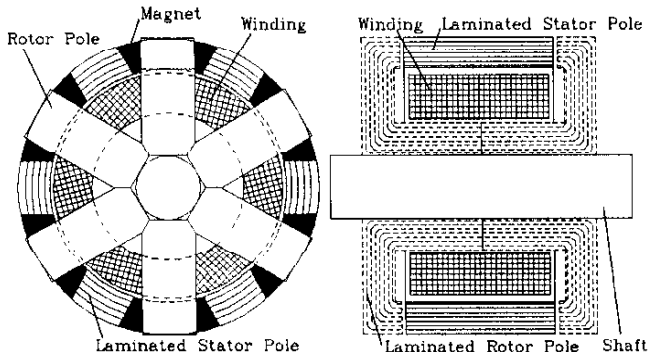

Fig. 3 An AFCC machine using laminated silicon-iron.

TABLE I
COMPARISON OF DESIGN FEATURES FOR VARIOUS MACHINE TOPOLOGIES

	End-winding portion	PMs	Flux focus-ing	Phase flux	Current
AFCC	None	Stationary	Yes	Bipolar	Bipolar
Induction	Large	None	No	Bipolar	Bipolar
SRM	Small	None	No	Unipolar	Unipolar
DSPM	Small	Stationary	Yes	Unipolar	Bipolar
FRM	Medium	Stationary	No	Bipolar	Bipolar
BLDCM	Medium	Rotating	No	Bipolar	Bipolar
CLAW	None	Rotating	No	Bipolar	Bipolar

II. SIZING EQUATION ANALYSIS

An approaches for developing a general-purpose sizing equation have been provided in [2] and [3]. The AFCC machine has a main flux that is axially oriented, thus the sizing equation for axial flux machine [3] can be applied:

$$P_R = \frac{1}{1+K_\phi}\frac{m}{m_1}\frac{\pi}{2}K_e K_i K_p \eta B_g A \frac{f}{p}(1-\lambda^2)\frac{1+\lambda}{2}D_o^3 \quad (1)$$

where

- K_ϕ ratio of electrical loading on the rotor vs. that on the stator.
- m number of phases of the machine.
- m_1 number of phases of each stator
- K_e back emf factor incorporating the winding distribution factor K_w and the ratio between the area spanned by the salient poles and the total air-gap area.
- K_i current waveform factor.
- K_p electrical power waveform factor.
- η machine efficiency.
- B_g flux density in the air gap.
- A total electrical loading (stator plus rotor).
- f converter frequency.
- p machine pole pairs.
- D_o diameter of the outer surface.
- λ ratio of the diameter of inner surface of the stator vs. that of the outer surface.

In order to compare the AFCC machine with traditional machines such as induction machines, the definition of the electric loading should reflect the fact that should two machines have the same electric loading and current level, the heat dissipation should be essentially the same. In an induction machine, assume the total number of conductors (including those in the rotor) is (N_b), each conductor carries a rms current of (I_{rms}), and the total current in the cross section is the $\Sigma I_{rms}=N_b*I_{rms}$. The electrical loading of an induction machine is then defined as

$$A = \frac{\sum I_{rms}}{\pi D_g} = \frac{N_b I_{rms}}{\pi D_g} \quad (2)$$

The total copper loss is (ignoring the end-winding)

$$P_{culM} = N_b I_{rms}^2 \rho \frac{L_e}{S_c} = \frac{N_b I_{rms}}{\pi D_g} I_{rms} \pi D_g L_e \rho \frac{1}{S_c}$$

$$= A I_{rms} \lambda_0 \rho \frac{1}{S_c} \pi D_o L_e \qquad (3)$$

where S_c is the cross section area of a conductor, D_g is the diameter of the air-gap, D_o is the outer diameter of the machine and L_e is the stack length. The factor λ_0 is defined as

$$\lambda_0 = \frac{D_g}{D_o} \qquad (4)$$

In an AFCC machine, assume there are (N_t) turns in the winding and carries a rms current of (I_{rms}). The total current on the cross section will be $\Sigma I_{rms}=2N_t*I_{rms}$. The total copper loss is

$$P_{cuAFCC} = N_t I_{rms}^2 \rho \frac{\pi D_g}{S_c} = \frac{2N_t I_{rms}}{2L_e} I_{rms} \lambda_0 \rho \frac{1}{S_c} \pi D_o L_e \quad (5)$$

where L_e is the total length of the machine without shaft, D_g is the average diameter of the winding and D_o is the outer diameter of the machine.

Hence, It is reasonable to define the electric loading for AFCC machine as

$$A = \frac{2N_t I_{rms}}{2L_e} = \frac{\sum I_{rms}}{2L_e} \qquad (6)$$

The copper loss of an AFCC machine will then have the same form as Eq.(3)

$$P_{cuAFCC} = A I_{rms} \lambda_0 \rho \frac{1}{S_c} \pi D_o L_e \qquad (7)$$

Eqs. (3) and (7) introduce the direct relationships between the copper losses and the electrical loading, current level, and overall size. Refering to the Eqs. (3) and (7), it is clear that, if the electrical loading for the AFCC machine is defined as Eq. (6), the copper losses of an AFCC machine and an induction machine are competitive. That is, if the two machines have the same electrical loading the copper losses of the two will be at the same level. It should be noted that, the end winding of induction machine has not been taken into consideration. Because there is no end winding in an AFCC machine, this definition of the electrical loading will clearly be favorable to the induction machines when making a comparison. Another issue is that the factor λ_0 for AFCC machines is not the same as that of induction machines. The term depends upon the size, pole number, speed, etc.

In the general case, as pointed out in an example later in this paper, the factor λ_0 is slightly smaller in AFCC machines than in induction machines. This fact is also favorable to the induction machine when doing a comparison. It is recognized that these expressions are approximate. However, deeper examination of the issues leads to a complicated theoretical approach and geometric analysis which is outside the scope of this sizing equation analysis.

For the same reason, the electric loading for axial flux machine has been defined in [2] as

$$A = \frac{\sum I_{rms}}{\pi D_g} = \frac{\sum I_{rms}}{\pi \frac{D_o + D_i}{2}} = \frac{\sum I_{rms}}{\pi \frac{(1+\lambda) D_o}{2}} \qquad (8)$$

In order to use the sizing equation (1), this expression should be adjusted by introducing Eq. (8) to Eq. (1)

$$P_R = \frac{1}{1+K_\phi} \frac{m}{m_1} \frac{1}{2} K_e K_i K_p \eta B_g \bullet$$

$$[A\pi \frac{(1+\lambda) D_o}{2}] \frac{f}{p} (1-\lambda^2) D_o^2$$

$$= \frac{1}{1+K_\phi} \frac{m}{m_1} \frac{1}{2} K_e K_i K_p \eta B_g \bullet$$

$$[\Sigma I_{rms}] \frac{f}{p} (1-\lambda^2) D_o^2 \qquad (9)$$

Then, introducing Eq. (6) to Eq. (9)

$$P_R = \frac{1}{1+K_\phi} \frac{m}{m_1} \frac{1}{2} K_e K_i K_p \eta B_g \bullet$$

$$[A\ 2\ L_e] \frac{f}{p} (1-\lambda^2) D_o^2$$

$$= \frac{1}{1+K_\phi} \frac{m}{m_1} K_e K_i K_p \eta B_g A \frac{f}{p} (1-\lambda^2) D_o^2 L_e \quad (10)$$

The average back emf is

$$E = \frac{d\Lambda}{dt}$$

$$= N_t \frac{d\theta}{dt} \frac{d\phi}{d\theta}$$

$$= N_t \frac{2\pi f}{p} 2 \bullet B_g \frac{K_m [\frac{\pi}{4}(1-\lambda^2) D_o] / 2}{2\pi / 2p}$$

$$= \frac{\pi}{2} p K_m N_t B_g \frac{f}{p} (1-\lambda^2) D_o^2 \qquad (11)$$

where Λ represents the phase flux linkage, N_t is the number of turns of the winding, K_m is the ratio of the area occupied by stator poles vs. the total area of stator end-surface.

$$K_m = \frac{\frac{\pi}{4}(1-\lambda^2)D_o^2}{2} - 2pL_{pm}\frac{(1-\lambda)D_o}{2} \qquad (12)$$
$$= \frac{\pi}{8}(1-\lambda^2)D_o^2 - pL_{pm}(1-\lambda)D_o$$

where L_{PM} represents the thickness of the PMs.

From Ref. [2], the back emf equation is

$$E = K_e N_t B_g \frac{f}{p}(1-\lambda^2)D_o^2 \qquad (13)$$

The factor K_e can be found as

$$K_e = \frac{\pi}{2}pK_m \qquad (14)$$

Thus for AFCC machines the power rating is

$$P_R = \frac{\pi}{2}\, pK_m K_i K_p \eta B_g A \frac{f}{p}(1-\lambda^2) D_o^2 L_e \qquad (15)$$

III Performance Analysis

For convenience of analysis and to permit use of optimization techniques, a linear model can be defined along the average diameter of the poles. Through a finite element analysis, the flux distribution for the maximum torque position has been calculated and is shown on Fig. 4. The torque curves calculated from the finite element analysis (FEA) are shown on Fig. 5. An optimization for the factor K_m was performed utilizing FEA and the optimized value was found to be in the range of 0.5 to 0.6. For a larger machine, the larger value of K_m can be selected. For a smaller machine, a smaller value K_m is preferable.

It should be mentioned that the large torque ripple shown in Fig. 5 is a common phenomena for converted fed machines (CFMs) including the claw-pole type or transverse flux type of machine. For applications such as traction drives where torque ripples are of concern, a multi-phase machine can be constructed by employing several identical AFCC machines on the same shaft. Each of those machines is shifted by an appropriate electrical angle. Also, the current modulation can be applied to minimize the torque ripple. Ideally, the AFCC machine is desired to have rectangular waveforms for current and back emf. In practice, due to the limits of manufacturing and the capability of converter, the machine will have a trapezoidal waveform. Simulations of current and voltage waveforms are shown on Fig. 6. Hence, the factor K_i

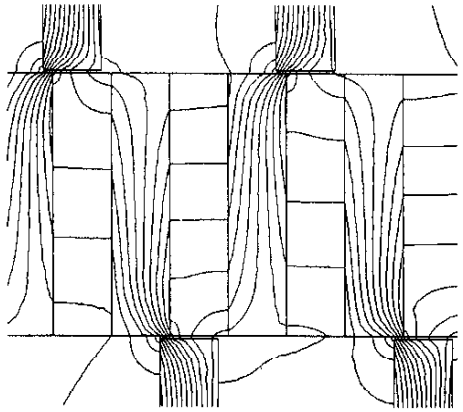

Fig. 4. Flux distribution in maximum torque position

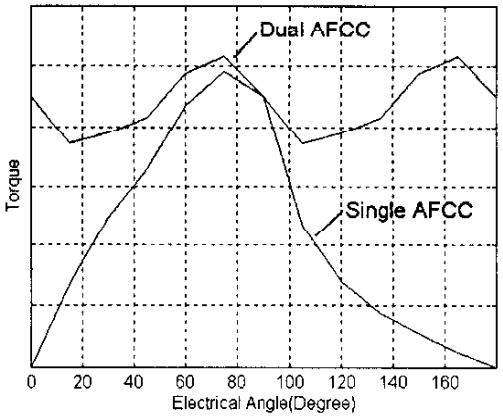

Fig. 5. Torque capability of AFCC

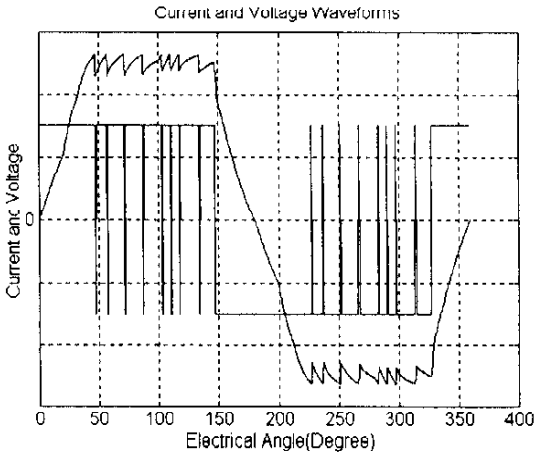

Fig. 6. The current and voltage waveforms

TABLE II

TYPICAL PROTOTYPE WAVEFORMS

Model	e(t)	i(t)	K_i	K_p
Sinusoidal waveform	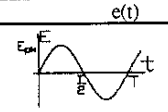	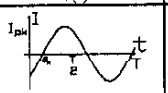	$\sqrt{2}$	$\frac{1}{2}\cos\phi$
Sinusoidal waveform	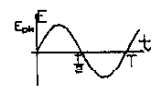	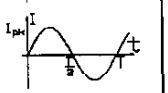	$\sqrt{2}$	0.5
Rectangular waveform	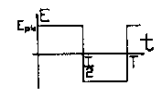	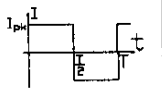	1	1
Trapezoidal waveform	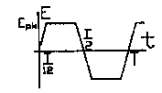	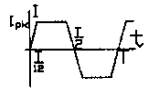	1.134	0.777
Triangular waveform	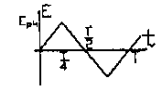	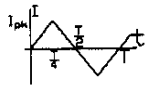	$\sqrt{3}$	0.333

and K_p defined in Ref. [1] will have the approximate values of 1.134 and 0.777, respectively. The actual values of these design factors will depend upon the converter capability for specific conditions. Table II shows different back emf and current waveforms and corresponding factors K_i and K_p.

IV. POWER DENSITY COMPARISON

The power density for an AFCC machine is defined as

$$\xi_{AFCC} = \frac{P_R}{\frac{\pi}{4} D_o^2 L_e} \tag{16}$$

From Ref. [1], the sizing equation of the induction machine is

$$P_{R(IM)} = \frac{\sqrt{2}\pi^2}{2(1+K_\phi)} K_w \eta \cos\phi_r B_g A \frac{f}{p} \lambda^2 D_o^2 L_e \tag{17}$$

and the power density is

$$\xi_{(IM)} = \frac{2\sqrt{2}\pi}{(1+K_\phi)} K_w \eta \cos\phi_r B_g A \frac{f}{p} \lambda^2 \frac{L_e}{L_t} \tag{18}$$

where K_w is the winding factor and L_t is the total length of the induction machine including end winding.

For a typical AFCC machine:

K_m=0.55, K_i=1.134, K_p=0.777, B_{ga}=1.8, λ_a=0.7.

while for a typical induction machine:

K_ϕ=0.95, $\cos\phi_r$=0.9, K_w=0.9, B_{gi}=1.1, λ_i=0.65, L_e/L_t =0.6.

Assuming that the two machines have the same efficiency (η), electrical loading (A) and speed (f/p):

$$\frac{\xi_{AFCC}}{\xi_{IM}} = \frac{\frac{\pi}{2} pK_m K_i K_p \eta B_{ga} A \frac{f}{p} (1-\lambda_a^2)}{\frac{\sqrt{2}\pi^2}{(1+K_\phi)} K_w \eta \cos\phi_r B_{gi} A \frac{f}{p} \lambda_i^2 \frac{L_e}{L_t}}$$

$$= \frac{\frac{\pi^2}{4} pK_m K_i K_p B_{ga} (1-\lambda_a^2)}{\frac{\sqrt{2}\pi^2}{(1+K_\phi)} K_w \cos\phi_r B_g \lambda_i^2 \frac{L_e}{L_t}}$$

$$= 0.4755p \tag{19}$$

This result indicates that a 12-pole AFCC machine (Fig. 3) (p=6) has about 2.85 times of the power density as an equivalent induction machine. Due to the nature of AFCC machine, if the pole number doubled, the power density is nearly doubled as well while the power density of an induction machine remains almost the same. Hence, the AFCC machine can have much higher power density as long as the manufacturing technology and application environments permit the use of as many poles as possible in the machine. The AFCC machine shares this feature with the transverse flux machine.

V. MODELING AND PROTOTYPING

In order to achieve practical results, the design and analysis of the AFCC machines should based on the fact that the flux paths are three-dimensionally distributed. With the help of three-dimensional finite element analysis (FEA) tools, the modeling can predict the results of torque, flux density, back emf, etc., with an acceptable accuracy. A three-dimensional FEA model is shown on Fig. 7. Fig. 8 shows the flux on the rotor. The flux path shown is from one rotor plate to another. Fig. 9 shows one stator pole and two adjacent PMs. The flux of the PMs enters the stator pole, becomes axially oriented and is focused to one side.

The major objective of prototyping was to design and construct a "proof-of-principle" AFCC machine to investigate the function and advantage of this type of machine, and also to verify the method and accuracy of the modeling process. Based on manufacturing convenience and availability of materials, it was decided to use solid steel to fabricate the stator and rotor. Sm-Co blocks are used as the magnets. The machine is designed to have 6 pole pairs. Hence, there are 6 poles on each side of the rotor, 12 steel blocks and 12 Sm-Co blocks in the stator, as shown on Fig. 10. It was also decided that, the rotor poles, stator poles and magnets all have the same length of arc (15°). The length of the air-gap was

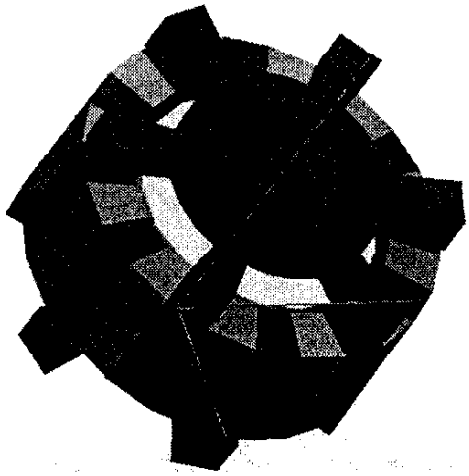

Fig. 7 A 3-D FEA model of an AFCC machine

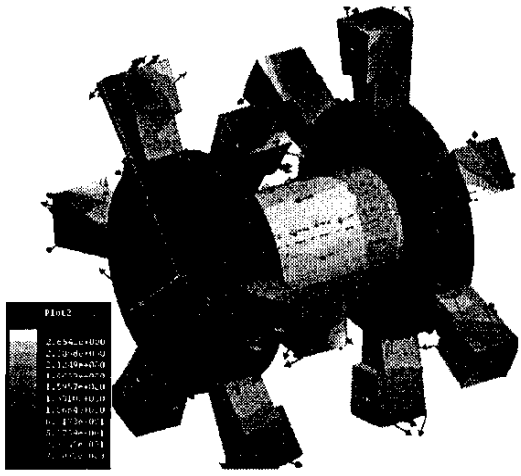

Fig.8 Flux in the rotor

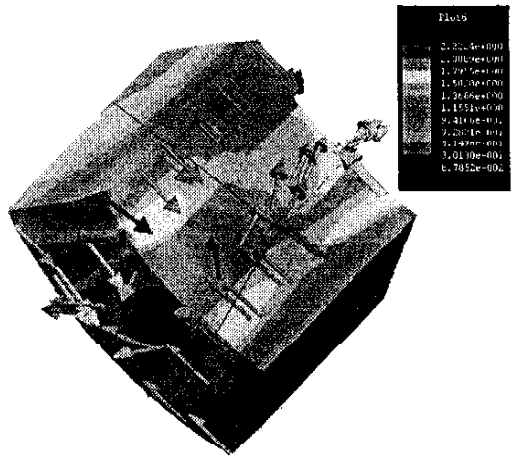

Fig. 9 Flux in a stator pole and two PMs

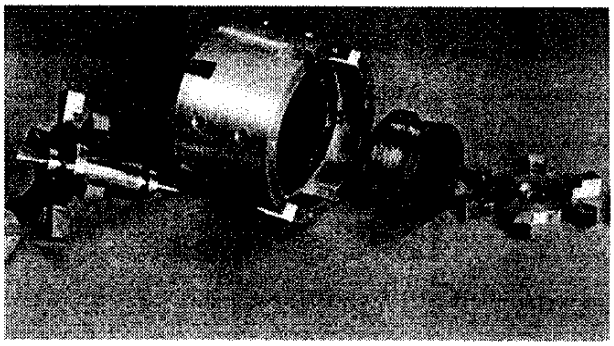

Fig. 10 The prototype of an AFCC machine

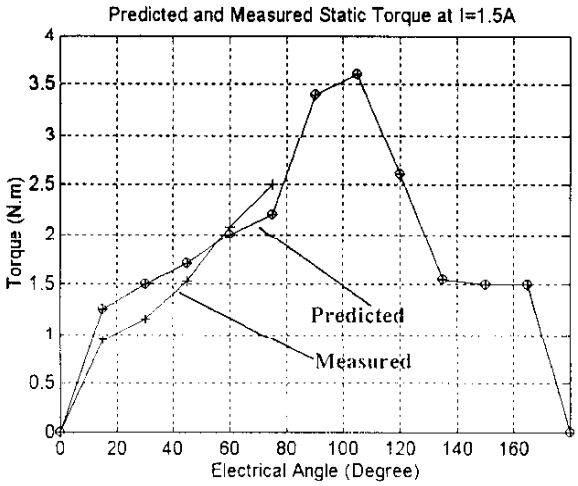

Fig. 11. Tested and predicted torque

designed to be 0.5 mm. However, it was enlarged to 1.5 mm to facilitate assembly and measurement. The prototype machine is shown on Fig. 10 and its specifications and test data are shown in Table III.

TABLE III
SPECIFICATIONS AND TEST DATA OF PROTOTYPE AFCC MACHINE

Magnet	SmCo5
Stator outer diameter (mm)	70.00
Stator inner diameter (mm)	50.00
Winding inner diameter (mm)	26.00
Air-gap (mm)	1.50
Total length (mm)	44.00
N_t	900
Pole pairs	6
K_m	0.5
Current (A)	1.5
B_g (T)	1.5
Average static torque (Nm)	1.21

For the AFCC machine, the average static torque is equal to the average dynamic torque if rectangular waveforms are achieved for current. Hence, the average static torque is then

$$T_s = \frac{P_R}{K_i K_p \omega} = \frac{1}{4} p K_m \eta B_g A (1-\lambda^2) D_o^2 l_e \quad (20)$$

where ω is the angular speed.

Introducing the prototype specifications and Eq. (15) to Eq. (20), for the prototype,

K_m=0.5, B_{ga}=1.1, λ_a=0.7

The average static torque predicted by the sizing equation is 1.1 Nm. The torque-angle curve is provided by FEA. The predicted curves (obtained by FEA) and tested torque curves are shown in Fig. 11. The test data shows that the maximum torque (2.5 Nm) point occurs at approximately 75 degrees, while the FEA predicts a maximum (3.6 N.m) at 105 degrees. The average predicted static torque is 1.75 Nm while the measured value is roughly 1.21 Nm, close to the value predicted by the sizing equation.

It is also interesting to compare the prototype to a commercial product of an induction machine. That is a ¼ HP motor, rated speed is 1755 rpm. The rated torque will then be 1 Nm. The frame size is NEMA 48. If the prototype operates at same speed, the machine would have a trapezoidal waveform (K_i = 1.134). Hence the dynamic torque is obtained by dividing the static torque with factor K_i. Table IV provides the comparison of the two motors.

The ratio in Table IV is the comparison of the Torque/volume ratio. When comparing the power density of the two machines, it is necessary for them to operate at the same speed. Hence the ratio is also the power density ratio for two machines compared at the same operating speed.

Referring to the discussion concerning electrical loading, it is also interesting to examine the factor λ_0. From the specification of the prototype, it can be found that the average diameter of the winding is (50+26)/2=38 mm. Hence the factor

$$\lambda_0 = 38/70 = 0.54 \quad (21)$$

while in induction machines the factor λ_0 is about 0.6 to 0.7. This result indicates that the definition of electrical loading that has been used is reasonable. Also it is again slightly favorable to induction machines when making a comparison.

TAB IV
COMPARISON OF PROTOTYPE WITH A COMMERCIAL INDUCTION MOTOR

	AFCC	Induction
Outer Diameter (mm)	70	122
Total Length (mm)	44	44
Volume (mm^3)	169246	514093
A (A/cm)	138	
Torque (Nm)	1.07	1
Torque/Vol.(Nm/mm^3)	6.32-6	1.95e-6
Torque/Volume Ratio	3.27	1

VI. CONCLUSION

1. From the size equation analysis, it is found that the AFCC machine has higher power density than a traditional induction machine. As the pole number increasing, this advantage becomes increasingly apparent. For example, a 12-pole AFCC machine ideally has 2.8 times the power density of an induction machine. Later by comparing the prototype to a commercial induction machine, it is found that the power density (or torque density) of the prototype is about 3 times as the same as that of the induction machine.
2. The circumferential winding totally eliminates the end-winding portion of the machine. This will significantly reduce the amount of copper used in the machine, which not only reduces the cost, but also reduces the copper losses and stator leakage inductance. Considering that the copper losses may account as many as 80% of the total losses in many forced cooling induction machines, this advantage is clearly attractive.
3. By placing the poles with different polarities on the opposite sides of the machine, the pole-to-pole leakage, a severe problem with the TFM type machines and claw pole machines, is eliminated. Also, the flux focusing structure in the stator provides the application of inexpensive materials such as ferrite permanent magnets. At the same time, the structure of the machine remains reasonably simple and the use of traditional laminated silicon-iron would make the manufacturing cost acceptable.
4. The torque ripple of the AFCC machine has been identified as the major drawback with this machine. The situation can be improved by introducing several identical machines on the same shaft. Although additional machines could be introduced, two machines coupled on the same shaft would appear to provide an optimized structure. Use of the proper winding arrangement provides the possibility of using this twin machine structure with either a two or three phases. To further improve the torque ripple, current modulation can be employed as has been successfully demonstrated for SRMs.

5. By constructing and measuring a prototype of the AFCC machine, the accuracy and reliability of modeling method has been verified. The impact of iron losses on this machine and it alleviation will be discussed in a future paper.

REFERENCES

[1] T. A. Lipo and Y. Li, "The CFM: A New Family of Electrical Machines", Conf. Rec. IPEC (Japan), April 3-7, 1995, pp. 1-8 (keynote paper).

[2] S. Huang, J. Luo, F. Leonardi, and T. A. Lipo, "A General Approach to Sizing and Power Density Equations for Comparison of Electrical Machines", *IEEE Trans. on Industry Applications*, vol. 34, No. 1, Jan./Feb., 1998, pp. 92-97,

[3] S. Huang, J. Luo, F. Leonardi, and T. A. Lipo , "A Comparison of Power Density for Axial Flux Machines Based on General Purpose Sizing Equations", *IEEE Power Engineering Summer Conference*, July 1997, Berlin, Germany. (to appear in PES Transactions).

[4] P. J. Lawrenson, J. M. Stephenson, N. N. Fulton, P. T. Blenkinsop, J. Corda, "Variable speed switched reluctance motors", IEE-Proceedings-B-(Electric-Power-Applications).vol.127, no.4, July 1980, p.253-6.

[5] Y. Liao, F. Liang, and T. A. Lipo, "A Novel Permanent-magnet motor with doubly-salient structure," *IEEE Trans. On Industry Applications* vol 31, Sept/Oct. 1995, pp. 1069-1078,.

[6] Y. Li, F. Leonardi and T. A. Lipo, "A Novel Doubly Salient Permanent Magnet Generator Capable of Field Weakening", *Conference on Design to Manufacture in Modern Industry (DMMI)*, Lake Bled, Slovenia, May 29-30, 1995

[7] A. G. Jack, B. C. Mecrow, C. P. Maddison; N. A. Wahab, "Claw pole armature permanent magnet machines exploiting soft iron powder metallurgy", 1997 IEEE International Electric Machines and Drives Conference Record, May 1997, Milwaukee,WI,v+734 pp.MA1/5.1-3.

[8] H. Weh, "On the Development of Inverter Fed Reluctance Machines for High Power Densities and High Outputs", *etz Archiv*, Bd. 6, 1984, pp. 135-144 (In German).

[9] S. Huang, J. Luo and T. A. Lipo , "Analysis and Evaluation of the Transverse Flux Circumferential Current Machine", *IEEE-IAS Annual Conference Record*, Oct. 1997, New Orleans, Louisiana, pp. 378-384.

[10] R. Deodhar, S. Anderson, I. Boldea, and T. J. E. Miller, "The Flux Reversal Machine: A New Brushless Doubly-Salient Permanent-Magnet Machine", *IEEE Trans. On Industry Applications* vol 33, No. 4, July/August 1997, pp. 925-934.

Jian Luo (S'96) was born in Chengdu, China. He received his B.E. degree from Tsinghua University, Beijing, China, in 1984, and then M.E. degree from the First Academy of Aerospace Industry, Beijing, China, in 1987, both of electrical engineering. After that, he worked as an electrical engineer in Beijing Institute of Control Device, Beijing, China. He has been a Ph.D. student at the University of Wisconsin-Madison since 1995. His area of interest includes optimized electrical machines, drive design, modeling and simulation.

Dinyu Qin was born in Wuxi, China. He received the B.E. degree from Tsinghua University, Beijing in 1990, and the M.S. degree from the University of Wisconsin-Madison in 1996. From 1990 to 1995, he worked for the Wuxi Electrical Machine Plant, Wuxi, China. He is presently a Ph.D. student at UW-Madison. His interests span electric machine design, control and power electronics.

Thomas A. Lipo (M'64-SM'71-F'87) is a native of Milwaukee, WI. From 1969 to 1979, he was an Electrical Engineer in the Power Electronics Laboratory, Corporate Research and Development, General Electric Company, Schenectady NY. He became Professor of Electrical Engineering at Purdue University, West Lafayette, IN. in 1979, and in 1981 he joined the University of Wisconsin, Madison, in the same capacity, where he is presently the W. W. Grainger Professor for Power Electronics and Electrical Machines. Dr. Lipo has received the Outstanding Achievement Award from the IEEE Industry Applications Society, the William E. Newell Award of the IEEE Power Electronics Society, and the 1995 Nicola Tesla IEEE Field Award from the IEEE Power Engineering Society for his work. Over the past 30 years he has served IEEE in numerous capacities including President of the Industry Application Society.

Shuxiang Li is a native of Nantong, Jiangshu province, China. He received his BE degree of electrical engineering from Harbin Institute of Technology, Harbin, China, in 1960. After that, He worked at Beijing Institute of Control Devices as an electrical engineer, research fellow and professor. His research interests include permanent magnet motors, actuators, sensors and drive/measurement systems.

Surong Huang was born in Shanghai, China, He received the B.S., M.S. degrees in the electrical engineering from Shanghai University, Shanghai, China. From 1995 to 1996, he worked as a visiting faculty at the University of Wisconsin-Madison. At present, he is an Associate Professor, College of Automation, Shanghai University, Shanghai, China. His research interests are motor and drive design, power electronics and power systems.